de Haas–van Alphen effect measurements of the exchange energy and spin-scattering anisotropy in the Kondo alloy copper-iron[*]

H. G. Alles[†] and R. J. Higgins[‡]

Physics Department, University of Oregon, Eugene, Oregon 97403

(Received 13 June 1973)

Unequal scattering of conduction electrons of opposite spin in Cu from Fe impurities has been measured using the wave shape of the de Haas–van Alphen (dHvA) effect. Exchange coupling to the impurity and spin-scattering anisotropy lead to a shift in the relative amplitudes and phases of the harmonics expressed by the Lifshitz-Kosevich formalism of the oscillatory magnetization. Waveform analysis of the dHvA signal from the neck orbit in Cu-93-ppm Fe yields values of the exchange coupling energy which scale linearly with applied field over a range of 30–45 kG, a magnitude equivalent to a g-factor shift of 8% (antiferromagnetic) from pure Cu, and no observed temperature dependence over 1–2 °K. The spin-scattering anisotropy amounts to about 30% (with electron moment antiparallel to H more strongly scattered), and also shows linear-in-H T-independent behavior. Techniques are described to correctly make precise waveshape measurements, even in the presence of skin-depth effects.

I. INTRODUCTION

The nature of conduction-electron interaction with magnetic impurities has been investigated by examining a variety of macroscopic properties (resistance, susceptibility, etc.) and microscopic properties (NMR, Mössbauer effect, etc.).[1] Macroscopic properties provide a measure of the averaged interaction of all the conduction electrons on the Fermi surface with the magnetic impurity. These measurements have the advantage of being easier to make than microscopic measurements (in general) and the physical property of interest is measured in a direct manner. However, relating the measured property to fundamental properties is quite difficult owing to the averaging processes. Microscopic measurements, on the other hand, are more difficult to make, but the measured quantities are more directly related to fundamental properties which are calculated from simple models.

Landau quantum oscillations of the magnetic susceptibility [the de Haas–van Alphen effect (dHvA)] can be used to measure very specific properties of the impurity-electron interaction. The dHvA effect is produced by the electrons on a very narrow region of the Fermi surface, and often the wave functions of these electrons may be calculated to high precision. Since the applied field polarizes the spin of the conduction electrons, information about the spin-dependent part of the interaction can be deduced. A good deal of recent work using the dHvA effect has been directed toward the magnetic-impurity problem. For example, Lowndes *et al.* made scattering maps over the Fermi surface in Au-Fe as a function of temperature, and found strongly temperature-dependent scattering which depended on the part of the Fermi surface sampled.[2]

One of the more striking dHvA effects observed in a magnetic alloy was a "beat" in the dHvA amplitude in Cu-Cr as a function of the applied magnetic field.[3] Coleridge *et al.*[4] (CST) have extended these measurements to several other Kondo systems, and have developed a spin-split-zero technique to deduce the exchange energy between specific conduction-electron orbits and the magnetic impurity. They have also been able to infer a spin-dependent conduction-electron scattering rate [spin scattering anisotropy (SSA)] in some alloys which show a spin-split minimum rather than a complete zero.

Spin-split zeros (or minima) are a powerful tool for investigating the magnetic-impurity problem, but their use is limited to cases where spin-split zeros exist, and investigations are limited to the specific orientation where a zero occurs. In general, this is not a symmetry direction, and leads to experimental and theoretical complications. Additionally, the SSA must be small compared to the exchange energy or else the spin zero will disappear before an appreciable shift occurs. Finally, some orbits and systems of interest show no spin-split minima for any orientation.

II. WAVESHAPE ANALYSIS

A more general method of investigating the details of magnetic-impurity effects that does not require a coincident spin-split zero is analysis of the harmonic content and phase of the dHvA signal. Information about the g factor and SSA is contained in the waveshape of the dHvA effect. Consider the four most dominant contributions to the observed dHvA effect: the spin-up and spin-down (σ is the spin index) amplitudes for the first and second harmonic M_r^σ. Generalizing the Lifshitz–Kosevitch (LK)[5] formalism, M_r^σ may be expressed as

$$M_r^\sigma = \frac{-DH^{1/2}x_r}{r^{3/2}\sinh x_r}\, e^{-\alpha r X^\sigma / H}$$

$$\times \sin\left[2\pi r\left(\frac{F}{H}-\gamma\right) - \sigma\frac{r\pi m^* g'}{2m} \pm \frac{\pi}{4}\right] ,\qquad (1)$$

where D is a geometric amplitude term, $x_r = r\alpha T/H$, $\alpha = (m^*/m)\times 146.9$ kG°K^{-1}, m^* is the effective mass, X^σ is the scattering temperature, F is the oscillation frequency, γ is the zero-point phase term, $\sigma\pi m^* g'/2m$ is a phase shift (in $1/H$) due to the Zeeman spin splitting [σ is interpreted as $+1$ for spin up (moment down) and -1 for spin down (moment up)], g' is the effective g factor, and $\pm\pi/4$ is a geometrical phase factor, being minus (plus) for an orbit which is a maximum (minimum) extremal area.

A more convenient amplitude $\bar{M}_r^\sigma$ may be defined in terms of M_r^σ,

$$\bar{M}_r^\sigma = \frac{r^{3/2}\sinh x_r}{DH^{1/2}x_r}\, M_r^\sigma = e^{-r\alpha X^\sigma/H} . \qquad (2)$$

Suppose that X^+ (spin up) is X^0, and X^- (spin down) is $X^0 + \delta_X$, where δ_X is a measure of the SSA. Then

$$M_r^\sigma = \begin{cases} B \text{ for first dHva harmonic, spin up} \\[4pt] BA \text{ for first dHvA harmonic, spin down} \\[4pt] B^2 \text{ for second dHvA harmonic, spin up} \\[4pt] B^2A^2 \text{ for second dHvA harmonic, spin down,} \end{cases} \qquad (3)$$

where

$$B = e^{(-\alpha X^0/H)} , \qquad (4)$$

$$A = e^{-\alpha\delta_X/H} .$$

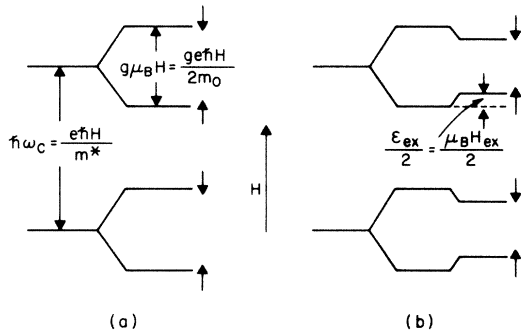The spin-up and spin-down contributions to the two harmonics will be out of phase (in $1/H$) with

FIG. 1. (a) Zeeman splitting of the Landau levels by the applied field H. The arrows across from each level signify the electron moment relative to the field direction. (b) Zeeman splitting as modified by the impurity exchange field H_{ex} or (equivalently) exchange energy E_{ex} (after Coleridge et al., Ref. 4).
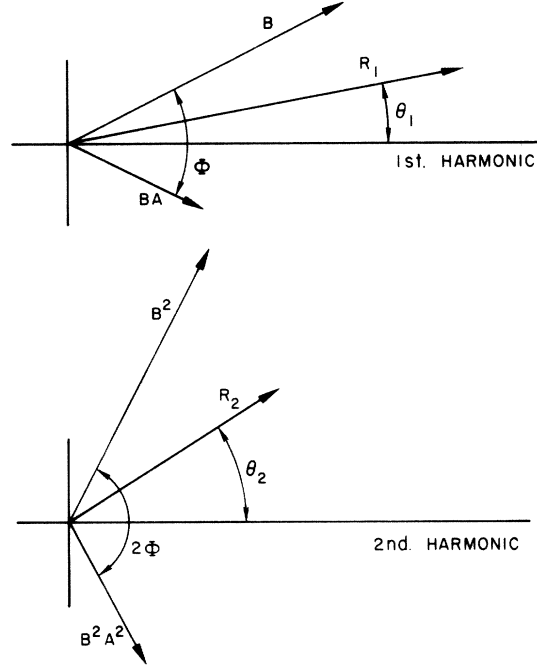

FIG. 2. Phasor diagram of the first- and second-dHvA-harmonic amplitudes defined in Eq. (3) in the presence of spin scattering anisotropy. Φ is the spin splitting angle, and θ_1 and θ_2 the SSA-induced phase shifts from the Lifshitz—Kosevich (horizontal axes) values.

each other by an amount Φ and 2Φ, where

$$\Phi = g'(m^*/m)\pi . \qquad (5)$$

g' is an effective g factor which is modified by the exchange energy ϵ_{ex} coupling conduction electrons to the impurity

$$g' = g - \epsilon_{ex}/\mu_B H = g - H_{ex}/H , \qquad (6)$$

where H_{ex} is defined as the exchange field.[3] The exchange interaction modifies the Landau-level spacing via an antiferromagnetic interaction, as illustrated in Fig. 1.

The components can be conveniently combined into first- and second-harmonic resultants R_r using the phasor diagrams in Fig. 2 [where the $\pi/4$ term in Eq. (1) has been suppressed]. Since the up and down components are unequal, the resultants suffer a phase shift of θ_r.

Elementary trigonometric manipulations produce the following relations:

$$R_1 = B(1 + A^2 + 2A\cos\Phi)^{1/2} ,$$

$$R_2 = B^2(1 + A^4 + 2A^2\cos2\Phi)^{1/2} ,$$

$$\theta_1 = \tan^{-1}\left(\tan(\tfrac{1}{2}\Phi)\frac{(1-A)}{(1+A)}\right) ,$$

$$\theta_2 = \tan^{-1}\left(\tan(\Phi)\frac{(1-A^2)}{(1+A^2)}\right) \quad . \tag{7}$$

The values of θ_1 and θ_2 cannot, in general, be measured directly without measuring the *absolute* phase, but their relative difference may be measured simply. Consider a window of several cycles of the dHvA signal beginning at some arbitrary field H_0. The first- and second-harmonic amplitudes may be represented as

$$R_1'(x) = R_1 \sin[2\pi F(x+\gamma') + \theta_1''] \quad ,$$

$$R_2'(x) = R_2 \sin[4\pi F(x+\gamma') + \theta_2''] \quad ,$$

where

$$x = 1/H - 1/H_0, \quad \gamma' = 1/H_0 - \gamma/F \quad ,$$

and

$$\theta_r'' = \theta_r \pm \pi/4 \quad .$$

Here γ' represents the arbitrary phase of the window origin. The waveform may conveniently be decomposed into sine S_r and cosine C_r components within the coordinates of the window:

$$R_1'(x) = R_1[\cos(2\pi F\gamma' + \theta_1'')\sin(2\pi Fx)$$

$$+ \sin(2\pi F\gamma' + \theta_1'')\cos(2\pi Fx)]$$

$$= S_1 \sin(2\pi Fx) + C_1 \cos(2\pi Fx) \quad ,$$

$$R_2'(x) = R_2[\cos(4\pi F\gamma' + \theta_2'')\sin(4\pi Fx)$$

$$+ \sin(4\pi F\gamma' + \theta_2'')\cos(4\pi Fx)]$$

$$= S_2 \sin(4\pi Fx) + C_2 \cos(4\pi Fx) \quad .$$

Thus, the measured phases θ_1' and θ_2' in this arbitrary window are

$$\theta_1' \equiv \tan^{-1}\left(\frac{C_1}{S_1}\right) = \tan^{-1}\left[\frac{\sin(2\pi F\gamma' + \theta_1'')}{\cos(2\pi F\gamma' + \theta_1'')}\right]$$

$$= 2\pi F\gamma' + \theta_1'' \quad ,$$

$$\theta_2' \equiv \tan^{-1}\left(\frac{C_2}{S_2}\right) = \tan^{-1}\left[\frac{\sin(4\pi F\gamma' + \theta_2'')}{\cos(4\pi F\gamma' + \theta_2'')}\right] \tag{8}$$

$$= 4\pi F\gamma' + \theta_2'' \quad ,$$

and the quantity

$$2\theta_1' - \theta_2' = 2\theta_1'' - \theta_2'' = 2\theta_1 - \theta_2 \pm \pi/4$$

will be independent of the choice of the window origin so that absolute phase information is unnecessary.

As an illustration of SSA effects, Fig. 3 shows computed values of $2\theta_1 - \theta_2$ as a function of Φ for various values of δ_χ. For $-\pi/2 < \Phi < \pi/2$, the two limits of no SSA and total SSA (only one set of spins contributing to the dHvA signal) produce no phase shift. It is only for intermediate amounts of SSA that an effect can be seen. In this range of Φ, the phase shift is generally small since θ_1 and θ_2 shift
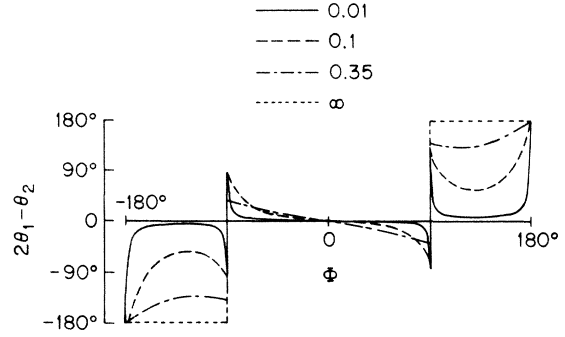

FIG. 3. Graphs of the SSA-induced change in the relative first- and second-harmonic phase $2\theta_1 - \theta_2 = (2\theta_1' - \theta_2')_{\mathrm{no\ SSA}} - (2\theta_1' - \theta_2')_{\mathrm{SSA}}$ versus Φ for several values of the SSA δ_χ, expressed in °K. The evaluation is for $m^*/m = 1$ and $H = 50$ kG. $(A = e^{-3\delta_\chi}.)$

in the same direction, and only the difference in the rate of shifts (caused by the second harmonic's much more rapid attenuation) produces the effect. However, if $\pi/2 < \Phi < \pi$ or $-\pi < \Phi < -\pi/2$, the phase shift is generally larger, since θ_1 and θ_2 shift in opposite directions. As δ_χ approaches ∞, the phase shift approaches π. For $\Phi = \pi/2$, the second harmonic will have a zero beat in the absence of SSA.

Since the amount of phase shift produced by a specific amount of SSA depends on Φ, the phase shift alone is not enough information to evaluate the SSA. The ratio R_2/R_1 is convenient to measure, and will also be strongly dependent on the SSA and Φ. Figure 4 demonstrates the effect of SSA on the quantity $\ln(R_2/BR_1)$ [Eqs. (4) and (7)], which is independent of X^0. With no Landau-level splitting ($\Phi = 0$) and no SSA, R_2/BR_1 equals 1. Variations from this value result from the interference between the dHvA signal from the spin-up and spin-down electrons. In the limit of total SSA, only one set of spins will contribute, and R_2/BR_1 will be 1 for all values of Φ.

The logarithmic derivative of R_2/R_1 with respect to $1/H$ provides an additional piece of information. In the absence of SSA, this quantity β is simply related to X:

$$\beta = \frac{d\ln(R_2/R_1)}{d(1/H)} = \alpha X \quad ,$$

with α as defined for Eq. (1).
   With SSA,

$$\beta = \left(R_1\frac{dR_2}{d(1/H)} - R_2\frac{dR_1}{d(1/H)}\right)\bigg/R_1R_2 \quad . \tag{9}$$

Note that the usual method of determining X is subject to error when there is SSA. The amount of error depends on the effective g factor and the
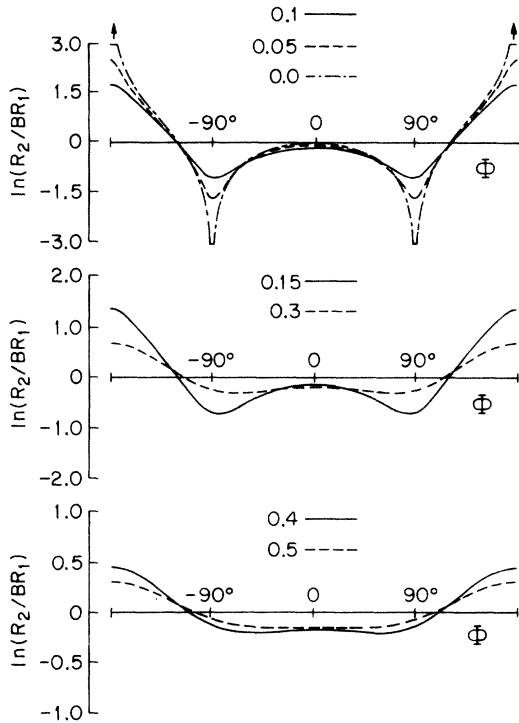
FIG. 4. Graphs of $\ln(R_2/BR_1)$ versus the Landau-level spacing Φ for various values of spin scattering anisotropy δ_X expressed in °K. The ratios are evaluated for $m^*/m = 1$ and $H = 50$ kG.

amount of SSA, and there is not enough information from a log plot of the first-harmonic amplitude to determine these quantities.

In general, for a magnetic-impurity system, the theoretical quantities (TQ) X^0, δ_X, and Φ must be considered field dependent, so that the measured quantities (MQ) $2\theta_1' - \theta_2'$, $\ln(R_2/R_1)$, and β will also be field dependent. The field dependence may be incorporated in equations describing the MQ in terms of the TQ to the same order in H as the MQ are known. This is described in the Appendix. A numerical-inversion routine may then be used to find values of the TQ which best reproduce the MQ.

III. EXPERIMENTAL CONSIDERATIONS

A. Waveshape analysis in Cu-Fe

Several considerations made Cu-Fe an ideal system to test dHvA waveshape analysis as a probe to study the magnetic-impurity interaction. The copper Fermi surface has been well determined and approximate wave functions of the conduction electrons of the various orbits have been calculated.[6] Very pure copper is easily attainable, and techniques for growing large single crystals of copper

have also been worked out in this laboratory.[7]

CST[4] have made dHvA scattering and spin-split-minimum measurements in Cu-Fe. Their results were limited to very low (~ 20 ppm) impurity content because the SSA was large enough to cause the spin-split zero to disappear before its position shifted significantly. However, their results do provide a comparison for the results of a waveshape analysis.

The neck orbit in copper is a particularly good choice for waveshape analysis. The orbit has a low frequency (2.17×10^7 G) and small effective mass ($0.46 m_0$), so the harmonic content is easy to measure. The orbit is also free of magnetic interaction (see latter discussion) over the field, temperature, and X range of interest. The effective mass and the g factor are such as to place Φ in the range where the phase shift of $2\theta_1' - \theta_2'$ is most sensitive to SSA.

For an Fe concentration of about 100 ppm, the belly-orbit amplitude is very much smaller than the neck's, so that only the neck signal is observed, even when harmonic-enhancement techniques (discussed later) are used. This greatly simplified the data analysis.

B. Sample preparation

A single crystal of Cu doped with Fe was prepared from a master alloy, and was grown using the Bridgeman technique.[8]

After growth, the crystal was cooled over a period of several hours to prevent thermal stress from damaging the crystal. It should be noted that the slow cooling may have introduced some clustering of the Fe atoms. Fe has a very low solubility in Cu, and a very rapid quench is needed to be absolutely certain that clustering does not occur. However, a rapid quench was not possible without introducing crystal damage unacceptable in dHvA amplitude studies.

Samples were acid cut from a portion of the slice free of subgrain boundaries and with a dislocation density of less than 5×10^4 cm^{-2}, to avoid background effects due to defects.[9]

Representative samples from the single crystal were analyzed using atomic-absorption spectroscopy.[10] The Fe concentration was found to be 93 ppm ($\pm 10\%$), in good agreement with the calculated concentration. Only one composition was used, and the sample will be referred to later as Cu-Fe for simplicity.

C. Experimental procedures

The dHvA data were taken using the field-modulation technique. A computer-centered automated system[11] was used to control all the experimental parameters (except temperature) and to process and store all the data. The temperature was sta-

bilized by a Cartesian diver within ±0.02 °K and measured using either a McLeod gauge or a precision manometer, depending on the temperature range.

The data consisted of a series of field windows (containing approximately seven dHvA cycles) spaced over the useful field range. Each window consisted of 256 high-resolution measurements spaced equally in $1/H$.

The two quadrature components of the first seven even harmonics of the modulation frequency were detected simultaneously using a software phase-sensitive detector (PSD).[12] In the discussions which follow, $n\omega$ will refer to detection at the nth harmonic of the modulation field.

Measurements were made in the temperature range of 1.2 to 4.2 °K, but only the data at and below 2.1 °K contained enough second dHvA harmonics to be of use in the waveshape analysis.

Only data on the [111] neck orbit were analyzed. The belly orbit with its larger effective mass $(1.37m_0)$ and higher X (~3 °K) had a signal too weak for reliable waveshape analysis. Further measurements in a more dilute alloy are in progress.

D. Modulation amplitude

The signal induced in the pickup coil using the field-modulation technique will be proportional to $\partial M/\partial t$, which may be written as[13]

$$\frac{\partial M}{\partial t} = -\sum_{r,\sigma} M_r^{\sigma} \sum_{n=1}^{\infty} 2n\omega \, J_n(\gamma_r)\sin(n\omega t + \tfrac{1}{2}n\pi) , \qquad (10)$$

where M_r^{σ} is defined in Eq. (1), $J_n(\lambda_r)$ is an integer-order Bessel function, and λ_r is the ratio of modulation amplitude to dHvA-oscillation-field spacing,

$$\lambda_r = 2\pi F_r h/H^2 , \qquad (11)$$

and where the modulation field may be written as $h\sin\omega t$.

The choice of modulation amplitude required considerable care, since the dHvA harmonic content could be greatly modified by the choice of λ_r. Since λ_r was constant for the data window (h adjusted proportional to H^2), the various $n\omega$ acted as a sort of coarse tuning, emphasizing different dHvA harmonics in different ω channels. Figure 5 shows the logarithm of the absolute amplitude of the first seven even-order Bessel functions as a function of λ. The log plot greatly distorts the familiar appearance of the Bessel function, but is useful to demonstrate its harmonic-enhancement abilities. λ for the second dHvA harmonic is twice as large as λ for the first harmonic. For $\lambda \ll n$, the Bessel functions are proportional to λ^n, so that the second harmonic is enhanced (relative to the first harmon-

ic) by a factor of 2^n (with a large signal loss), amounting to about 1.6×10^4 for 14ω. The harmonic content can also be increased by setting λ_1 near a zero for the nth Bessel function. This has an advantage over the $\lambda \ll n$ approach in that the signal level is not attenuated as much. The best approach for measuring the second-harmonic content is to adjust λ_2 to the first peak of an nth-order Bessel function, choosing n to provide the necessary enhancement. Under these conditions, the enhancement for 14ω is ~10^3, and drops very quickly with n to less than 10 for 4ω.

λ_1 was chosen as 4.9 for most of the data windows, and satisfied all of the above conditions for harmonic enhancement at various $n\omega$. The first Bessel zero is near λ_1 for 2ω. At 8ω, λ_2 is near the first Bessel maximum. For 10ω, 12ω, and 14ω, the power-law enhancement prevails.

E. Typical data

Figure 6 shows some typical data taken with the multiple-channel PSD and the corresponding Fourier transforms. The data shown (as well as four other channels) were taken simultaneously and demonstrates the enhancement of harmonic content possible with this technique. The data shown were taken at high field and low temperature, and have the most harmonic content of that measured. The range of LK second-harmonic content measured in the experiment was from about 4 to 0.02%.
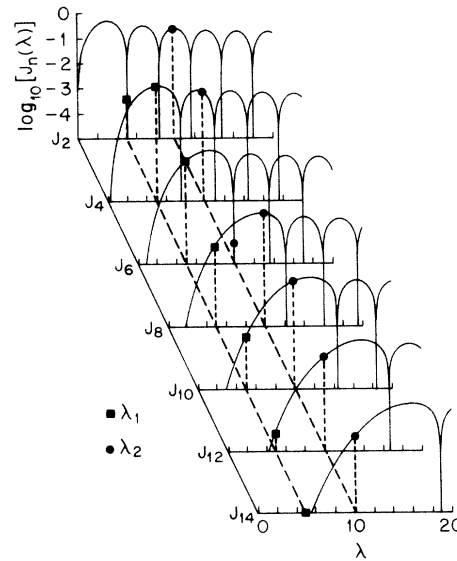
FIG. 5. Plots of $\ln(|J_n(\lambda)|)$ versus λ for the first seven even-order Bessel functions. The vertical axis corresponds to values of J_n from 10^{-5} to 1. All values less than 10^{-5} are plotted as 10^{-5}. The dashed lines show the values of λ_1 and λ_2 used in these experiments.

F. Skin-depth effects

The modulation field penetrating the sample and the dHvA signal propagating out of the sample are modified in amplitude and phase by induced currents. This can seriously affect precise dHvA amplitude and waveshape measurements.

The effects of a finite skin depth can be calculated explicitly for simple geometries and limiting conditions. A plane wave $\overline{W}$ propagating in a conductor becomes $\overline{W}e^{-kx}$, where $k = (1+i)/\delta$, x is the distance traveled in the conductor, and δ is the skin depth of the material given by $\delta = c/(2\pi\omega\sigma)^{1/2}$.

In the limit where δ is much smaller than the radius of the sample, the plane-wave approximation may be used, and the $n\omega$ dHvA signal S_n' generated a distance x from the surface will be modified so that

$$S_n' = S_n \frac{J_n(\lambda e^{-x/\delta})}{J_n(\lambda)} e^{ix/\delta},$$

where S_n is the unmodified signal. The $n\omega$ signal S_n'' seen outside the sample will be modified in the same way,

$$S_n'' = S_n' e^{-n^{1/2}x/\delta - in^{1/2}x/\delta},$$

where δ has been replaced by $\delta/n^{1/2}$ since the signal is at a n-times-higher frequency than the modulation signal. The total signal is found by summing this amplitude from all parts of the sample, and is proportional to a modified Bessel function (MBF) $J_n'(\lambda)$:

$$J_n'(\lambda) = \int_0^\infty J_n(\lambda e^{-z}) e^{-in^{1/2}z} e^{-i(1+n^{1/2})z} dz. \quad (12)$$

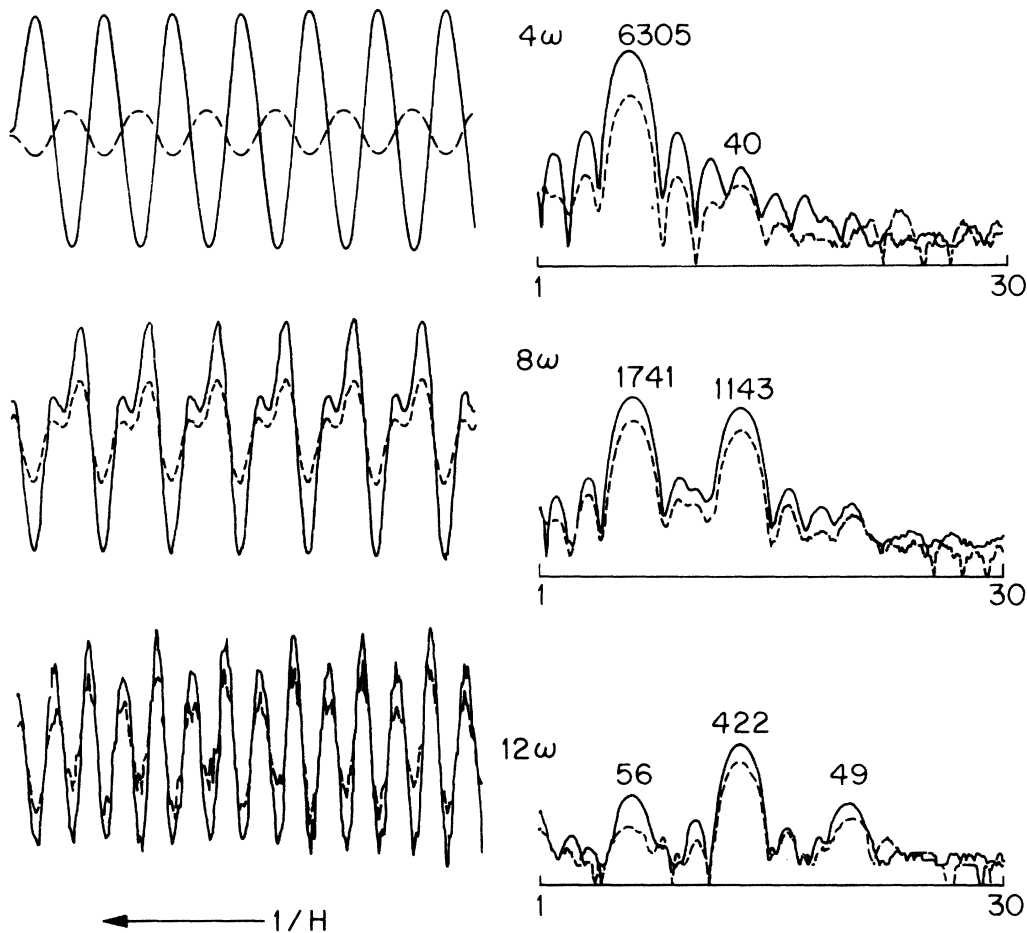This function[14] is complex, so that both in-phase

FIG. 6. dHvA data taken at 1.2 °K and 45 kG during a single field sweep using the multichannel software PSD. (A filter network was required to make each $n\omega$ signal comparable in amplitude.) The graphs to the left show the quadrature components detected at 4ω, 8ω, and 12ω. The graphs to the right show the log of the Fourier transform of the data. The numbers near the peaks are the relative amplitudes obtained in a Fourier decomposition fit to the data. The actual dHvA harmonic content for these data is about 4%.
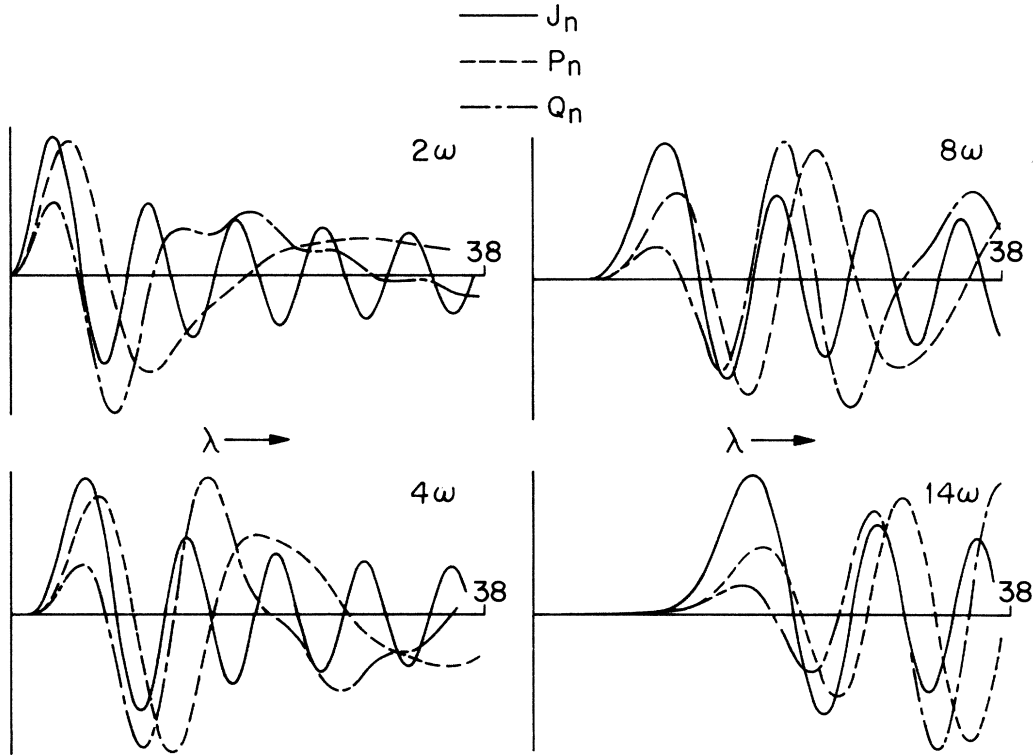
H. G. ALLES AND R. J. HIGGINS

—— J_n

———— P_n

—·—— Q_n

2ω

38

$\lambda \longrightarrow$

4ω

38

8ω

38

$\lambda \longrightarrow$

14ω

38

FIG. 7. Comparison between $J_n(\lambda)$ and $J_n'(\lambda) = P_n(\lambda) + iQ_n(\lambda)$ [see Eq. (12)] for $n = 2$, 4, 8, and 14. P_n and Q_n have been scaled by an arbitrary factor. This evaluation is for the skin depth much less than the sample diameter.

and out-of-phase components appear at the pickup coil. Figure 7 shows the real $P_n(\lambda)$ and imaginary $Q_n(\lambda)$ parts of $J_n'(\lambda)$ compared with $J_n(\lambda)$ for $n = 2$, 4, 8, and 14. Since $P_n(\lambda)$ and $Q_n(\lambda)$ have very different forms, the dHvA amplitudes and relative harmonic content will depend on detection phase. In any case, an error in measured harmonic content will be made if $J_n(\lambda)$ is used to calculate the effect of the modulation amplitude. Since the skin depth may vary with magnetic field, this may introduce a spurious field dependence to the measurements. [15]

The limit where the skin depth is equal to or larger than the sample radius can be solved in a similar fashion, using the solution of the electromagnetic wave equations in cylindrical coordinates. The results show a much smaller departure from simple Bessel dependence, being most noticeable as a shift in the zeros and the appearance of an out-of-phase component. The over-all amplitude is also attenuated.

One observed effect of the MBF is shown in Fig. 8. The four graphs are of different phase projections for one data window detected at 4ω. The waveshape is strongly dependent on detection phase.

Serious error in the waveshape analysis will occur unless the detection-phase-dependent part of

the MBF is taken into account. The dHvA signal S_n'' generated by the sample may be written as

$$S_n'' = \sum_r G_r [P_n(\lambda_r)\sin(n\omega t) + Q_n(\lambda_r)\cos(n\omega t)] ,$$

where G_r is the actual amplitude of the rth dHvA harmonic. The amplifying network will introduce a phase shift φ, and so the dHvA amplitudes $G_{r,n}^p$ measured by the in-phase channel and $G_{r,n}^q$ measured by the out-of-phase channel will be

$$G_{r,n}^p = G_r [P_n(\lambda_r)\cos\varphi + Q_n(\lambda_r)\sin\varphi] ,$$

$$G_{r,n}^q = G_r [Q_n(\lambda_r)\cos\varphi - P_n(\lambda_r)\sin\varphi] .$$

The quantity

$$[(G_{r,n}^p)^2 + (G_{r,n}^q)^2]^{1/2} = G_r [P_n(\lambda_r)^2 + Q_n(\lambda_r)^2]^{1/2} = G_r |J_n'(\lambda_r)|$$

(13)

is invariant of the phase shift φ. Problems arising from detection-phase setting or field-dependent phase shifts may be eliminated by using the square root of the sum of the squares (SRSS) of the signals detected in the quadrature channels as the amplitudes for further analysis.

G. Modified Bessel-function calibration

The values of the MBF $|J_n'(\lambda_r)|$ must be known in order to deduce the dHvA harmonic content, yet

this quantity is sample-shape-dependent, and the form of Eq. (12) is only appropriate for a semi-infinite medium. However, since it is the amplitude *ratios* which are needed, only the ratio $|J_n'(\lambda_1)|/|J_n'(\lambda_2)|$ is needed, and this can be measured simply. Since $\lambda_2 = 2\lambda_1$,

$$|J_n'(\lambda_2)| = |J_n'(2\lambda_1)| \, ,$$

and

$$\frac{M_1(\lambda_1, n)}{M_1(2\lambda_1, n)} = \frac{KM_1|J_n'(\lambda_1)|}{KM_1|J_n'(2\lambda_1)|} = \frac{|J_n'(\lambda_1)|}{|J_n'(\lambda_2)|} \, , \qquad (14)$$

where $M_1(\lambda, n)$ is the amplitude of the first dHvA harmonic as measured by the $n\omega$ detection channel, M_1 is the actual amplitude, and K is the arbitrary gain of the system.

Thus by taking two data windows at the same field value, one using twice the modulation amplitude as the other, the ratio of the modified Bessel functions for first and second harmonics is simply the ratio of first-harmonic amplitudes. This requires no absolute measurements, and any systematic errors cancel.

Copper has a large magnetoresistance. It is reduced by impurity content, but is still sizable for 93-ppm Fe. The changing skin depth causes the MBF also to be field dependent. This is demon-

strated in Fig. 9, showing the SRSS [Eq. (13)] dHvA signal as a function of modulation current measured at two field values. The 2ω channel shows the most variation between the two plots and the greatest difference between plots occurs for the larger modulation fields. Data taken at the higher field display more perfect zeros for all ω channels, consistent with an approach to a simple Bessel-function dependence due to the increase in skin depth with increasing magnetic field.

The measured field-dependent MBF's were used to find the actual harmonic content from the measured values.

H. Magnetic interaction

Since the electrons in the sample respond to B rather than to H, the sample's oscillatory magnetization can produce a waveshape distortion. This effect is known as magnetic interaction (MI).[16] In the waveshape analysis used in this study, it was important that the MI-induced harmonics be much smaller than the normal LK harmonic content.

Phillips and Gold[17] have worked out a formalism which provides a simple check for the presence of appreciable MI. The first effect of MI is to produce a second-harmonic contribution M_2^{MI} which is proportional to $(M_1/H)^2$ and out of phase with the
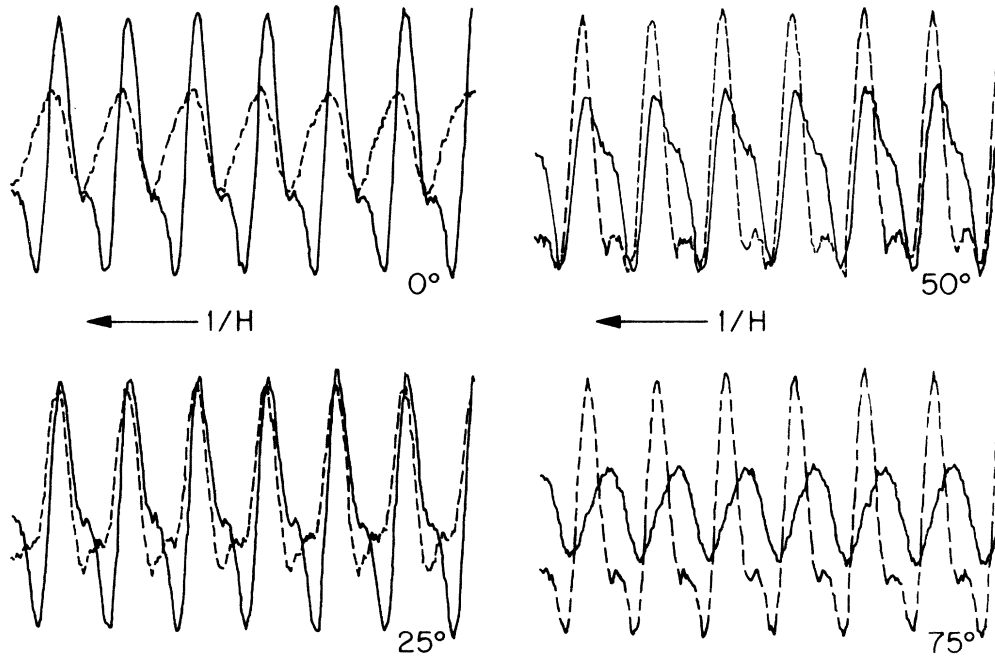

FIG. 8. Example of the effect of detection phase on the dHvA waveshape. Data were taken on the Cu—Fe sample with 100-Hz modulation frequency and 4ω detection at $1.2\,°$K and 45 kG with $\lambda = 9.8$. Each graph shows the two quadrature detection channels. The graph marked $0°$ is actual data while the graphs marked $25°$, $50°$, and $75°$ were computer generated from the data by doing a numerical phase rotation, equivalent to adjusting the phase setting of a conventional PSD.

LK second-harmonic contribution M_2^{LK}.[18] The ratio M_2^{MI}/M_2^{LK} is proportional to $T/H^{5/2}$ and is *independent* of the scattering temperature. Thus, the worst-case condition is at low fields and high temperatures (opposite to the worst-case MI conditions for conventional X measurements).

dHvA measurements were made on a pure-copper sample to determine how serious the MI contribution was for the neck orbit. The value of $2\theta_1' - \theta_2'$ [Eq. (8)] at 20 kG and 1.2 °K was 45° ± 0.5° [mod (π); see later discussion], equal to that expected for pure LK contribution. The absence of a phase shift placed an upper limit of 0.01 for the MI-to-LK ratio. The worst-case condition for the Cu-Fe measurements was 2.1 °K and 35 kG. For these conditions, the upper limit for the ratio was ~0.02. Thus, the Cu-Fe sample should have less than 2% MI contribution to the second-harmonic content for all temperatures and fields used in the experiment.

IV. RESULTS AND DISCUSSION

A. Data

Each of the 14 detected channels were decomposed into sine and cosine parts for the first and second dHvA harmonics using a Fourier decomposition program. Weighted averaging was then used to find the best values of θ_1', θ_2', and R_2/R_1 for each window [R_2/R_1 was corrected using the measured modified Bessel function; see Eq. (13)].

The results[19] of the measurements are shown in Figs. 10 and 11. Only the data at 1.23, 1.39, 1.6, and 2.1 °K had enough harmonic content to make a reliable analysis. Figure 10 shows the values of the relative phase $2\theta_1' - \theta_2'$ versus field. The error bars were assigned using the rms residuals from the Fourier decomposition and standard propagation of error analysis. The error is larger at lower fields owing to the decrease in second-harmonic amplitude. The limit of resolution for the second harmonic was about one part in 5000 of the first-harmonic amplitude, but only amplitudes larger than one part in 2000 were used in order to improve the reliability.

The $2\theta_1' - \theta_2'$ data fit a linear equation in H within experimental error. The use of higher-order H dependence did not improve the significance of the fit. Various π phase shifts in the experimental system introduce a π modularity in $2\theta_1' - \theta_2'$, and these are difficult to trace down. However, com-
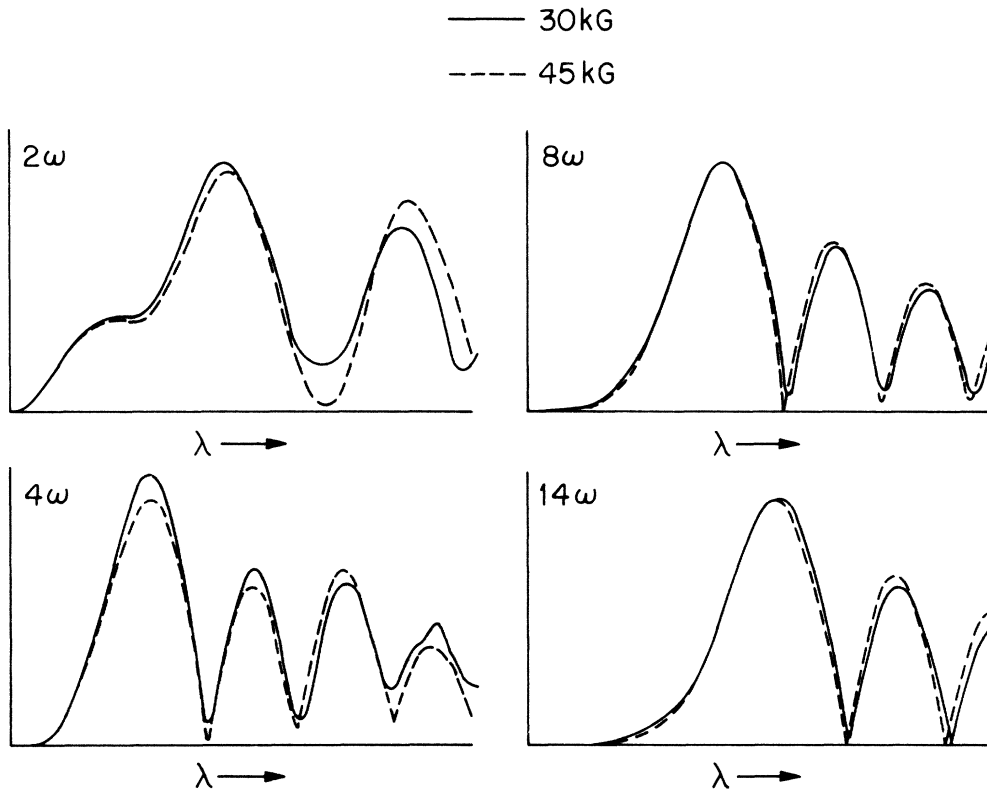

FIG. 9. dHvA amplitudes at constant field versus modulation amplitude. The traces on each graph were made at 30 and 45 kG. The scales have been adjusted to make the best least-squares agreement between the two sets of data. The plotted amplitude is the square root of the sum of squares of the signal in both quadrature channels.

parison with pure-Cu data taken under the same conditions allowed $2\theta_1' - \theta_2'$ *shifts* (i.e., $2\theta_1 - \theta_2$) to be determined modulo 2π. The Fe induced phase shift was found to be $\sim -105°$ when phasor diagrams of Cu and Cu-Fe were compared.

Figure 11 shows the values of $\ln(R_2/R_1)$ as a function of $1/H$, where R_1 and R_2 are defined by Eq. (7). The ratio R_2/R_1 was evaluated from the measured dHvA harmonic amplitudes M_1 and M_2 using the relation

$$\frac{R_2}{R_1} = 2\sqrt{2} \frac{|J_n'(\lambda_1)|}{|J_n'(\lambda_2)|} \frac{\sinh x_2}{\sinh x_1} \frac{x_1}{x_2} \frac{M_2}{M_1} , \tag{15}$$

where x_r is defined in Eq. (1) and the *measured* modified Bessel functions are used. The functional dependence of this ratio is

$$R_2/R_1 \propto e^{-\alpha \overline{X}/H} ,$$

where $\overline{X}$ is an effective scattering temperature. A logarithmic plot versus $1/H$ should then be a straight line for a field-independent $\overline{X}$. Although this has the same functional form as a conventional scattering temperature plot, it is fundamentally different. Any extraneous field-dependent amplitude due to skin-depth effects will be canceled out because a ratio of the harmonic amplitudes is used.

A linear equation in $1/H$ was fit to the data shown in Fig. 11. Higher-order equations in $1/H$ did not improve the significance of the fit. The apparent curvature at lower fields is not significant. Broad-

band noise in the data produced a contribution comparable to the second-harmonic amplitude at low fields, and thus made the ratio systematically too large.

Since $2\theta_1' - \theta_2'$ and $\ln(R_2/R_2)$ showed only first-order dependence on H, the field dependence could be accounted for by using values for only two different field points. Values of 30 and 45 kG were arbitrarily chosen as evaluation points since they covered the approximate range of the data.

B. Inversion results

The results of the numerical inversion to find the theoretical quantities are presented in Table I along with the corresponding measured quantities. The 30- and 45-kG values of X^0 and $X^0 + \delta_x$ are plotted in Fig. 12. This form of presentation is convenient to demonstrate the difference between spin-up and spin-down scattering. The error bars were estimated by allowing the deviations between the calculated and measured values of $2\theta_1' - \theta_2'$, $\ln(R_2/R_1)$, and β to be as large as the measurement uncertainty. The bars represent the absolute uncertainty of the quantities. The uncertainty of the scattering *difference* δ_x is about one-third as large.

The change in Φ caused by the magnetic impurities may be related to $\epsilon_{ex} = \mu_B H_{ex}$ by

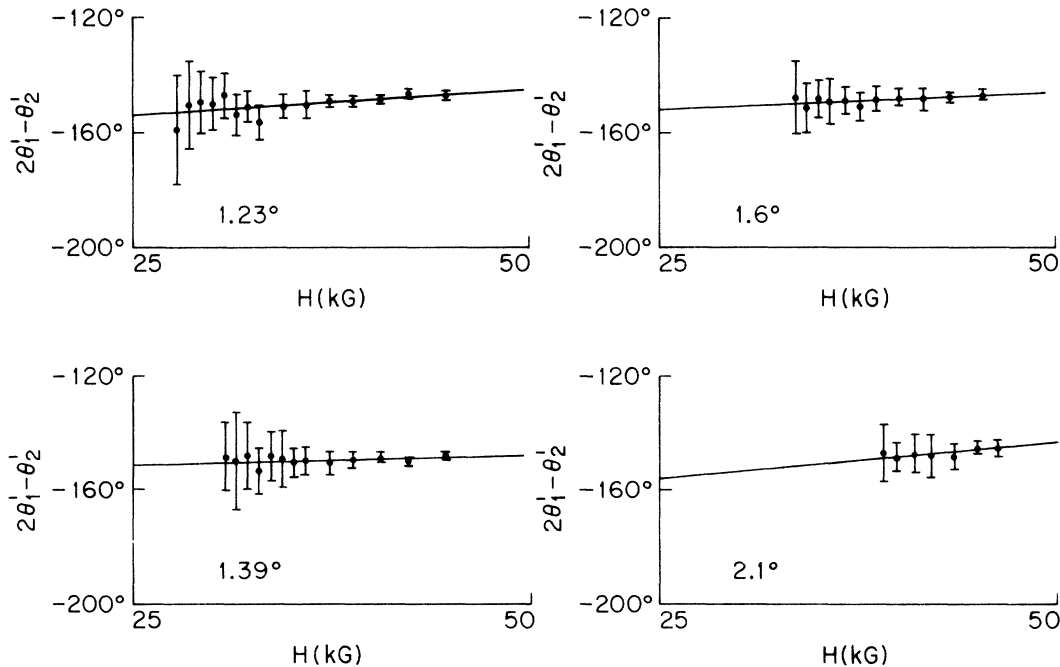$$H_{ex} = (m/\pi m^*)(\Phi_{Cu} - \Phi_{Cu\text{-}Fe})H . \tag{16}$$

FIG. 10. Measured values of $2\theta_1' - \theta_2'$ versus field in Cu-Fe for four different temperatures. The data show a difference of about $-105°$ from pure Cu $[(2\theta_1' - \theta_2')_{Cu} = -45°]$.
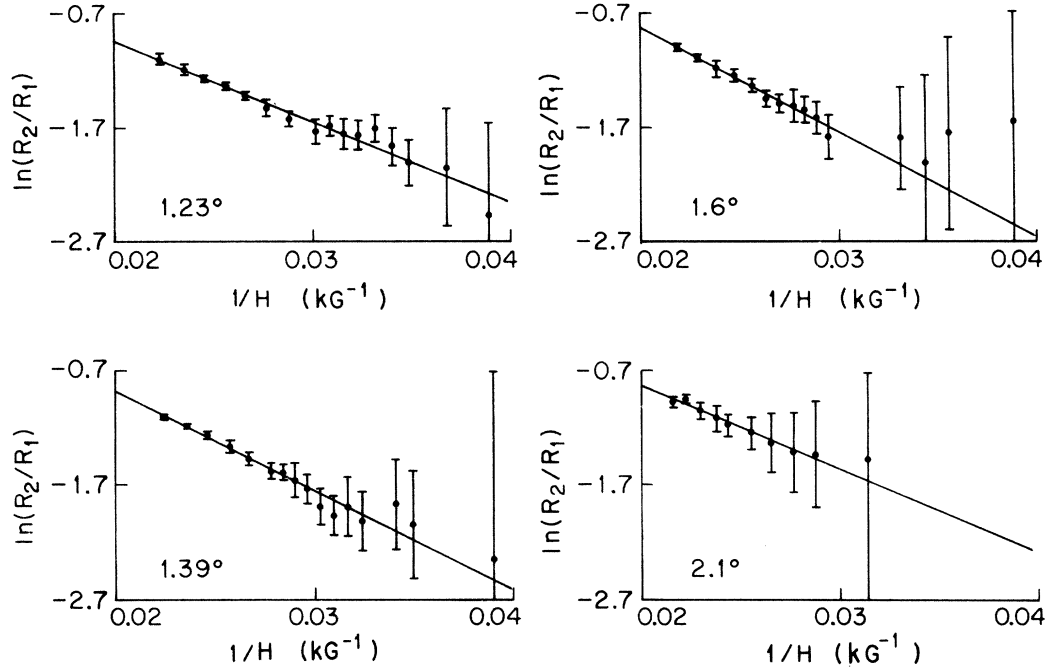
FIG. 11. Measured values of $\ln(R_2/R_1)$ versus field in Cu-Fe for four different temperatures. The vertical axis is the logarithm of the ratios measured in the 8ω channel. The values from the 2ω channel were similar.

Figure 13 shows the values of H_{ex} at 30 and 45 kG as a function of temperature. The uncertainty in the *difference* between 30- and 45-kG values is only about one-third as large as the error bars shown.

A straight-line fit to the values of each quantity at the four temperatures comes very close to passing through all the error bars, indicating that the variations with temperature are not very significant. The systematics of the variation are somewhat misleading since the equations are coupled.

Random variations would tend to produce common effects among X^0, δ_X, and H_{ex}.

Temperature-*independent* behavior in this temperature and field range is supported by measurements of several different physical properties. The impurity contribution to resistivity saturates around 2 °K, and lowering the temperature does not increase its contribution.[20] In Cu-Fe, the logarithmic increase in resistance associated with the Kondo effect occurs between about 5 and 15 °K. The

TABLE I. Tabulation of measured and calculated quantities measured in 93-ppm Cu-Fe. The various quantities are defined in the text. Values shown at 30 and 45 kG are the results of a linear fit to data spanning to field range.

|	1.23 °K		1.39 °K		1.60 °K		2.10 °K		Average		Approximate uncertainty
Field (kG)	30	45	30	45	30	45	30	45	30	45	
$2\theta_1 - \theta_2$ (deg)	−107.6	−102.0	−104.9	−102.7	−105.8	−101.9	−108.7	−100.8	−106.8	−101.9	±2°
$\ln(R_2/R_1)$	−1.86	−1.09	−2.04	−1.09	−1.91	−0.96	−1.79	−0.99	−1.90	−1.03	±0.1
$-(1/\alpha)\beta$ (°K)	1.02		1.26		1.26		1.06		1.14		±0.1
$\Phi_{Cu} - \Phi_{Cu\text{-}Fe}$ (deg)	12.6	12.6	11.8	11.4	9.9	9.0	11.3	11.7	11.4	11.2	±1.5
H_{ex} (kG)	4.55	6.80	4.25	6.15	3.70	4.90	4.05	6.30	4.14	6.04	±0.8
X^0 (°K)	1.09	1.14	1.18	1.16	1.15	1.13	1.07	1.09	1.12	1.13	±0.08
δ_X (°K)	0.28	0.38	0.26	0.37	0.23	0.34	0.27	0.36	0.26	0.36	±0.03
$X^0 + \delta_X$ (°K)	1.37	1.52	1.44	1.53	1.38	1.47	1.34	1.45	1.38	1.49	±0.1
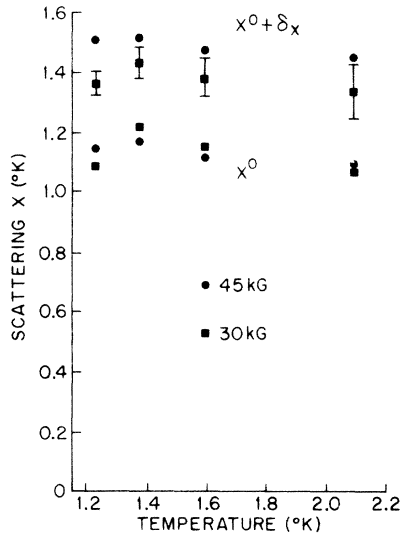
FIG. 12. Scattering temperature for spin up $(X^0 + \delta_\chi)$ and spin down (X^0) electrons as a function of temperature at 30 and 45 kG. The error bars for all four points at a given temperature are equal. However, the error bars for δ_χ are about $\frac{1}{3}$ as large as for X^0.

same temperature dependence of the resistance is seen in fields of 20 kG, the only difference being a reduction of the saturation value by about 3%.[21] Mössbauer studies of the Fe hyperfine field also show no temperature dependence in the 1 to 2 °K range up to fields of 60 kG.[22]

FIG. 14. Phasor diagram of the dHvA spin components deduced from the Cu-Fe measurements at 45 kG. In this diagram $B = 0.165$ and $A = 0.58$ [see Eq. (4)]. The relative scale between the first- and second-harmonic diagrams is arbitrary. The dashed lines represent the reference phases measured in pure Cu. The 45° relative phase for the second harmonic is the value given in the Lifshitz−Kosevich theory. This value was obtained (as a check on the measurements) in a separate experiment on pure Cu.
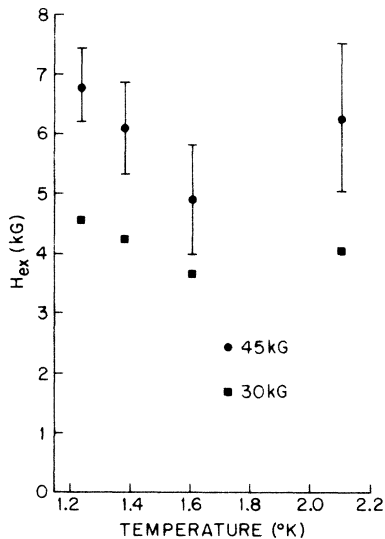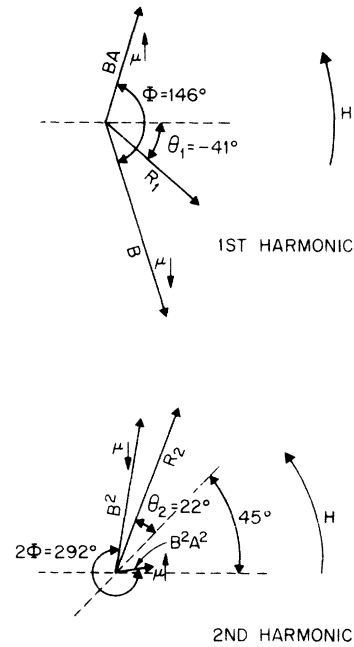

FIG. 13. Exchange field H_{ex} as a function of temperature at 30 and 45 kG. The error bars at 30 and 45 kG are equal, and represent the absolute error. The uncertainty of the difference between the 30 and 45 kG values is about 25% less than the error bars shown.

The variations with temperature are much smaller than the magnitude of the quantities and should not influence the general interpretation of the results. For the purposes of the remaining discussion, the average of the values shown in Table I will be used.

The ratios of H_{ex}/δ_χ at 30 and 45 kG are equal within 5%. If H_{ex} and δ_χ are assumed to be zero for $H = 0$, the 30- and 45-kG values of δ_χ and H_{ex} are consistent with a linear field dependence.

Since H_{ex} is proportional to H, the effective g factor g' defined by Eq. (6) will be independent of H. The Fe impurity simply introduces a field-independent change in the g factor as seen by the dHvA effect. Thus, a beat in the dHvA amplitude as a function of the field as seen in Cu-Cr[3] cannot occur in Cu-Fe. Figure 14 is a phasor diagram showing the analysis of the signal measured in Cu-Fe at 45 kG. The dashed lines designate a reference phase in the LK theory in the absence of a magnetic impurity (and MI effects), and as measured in pure Cu.

Careful analysis of the diagram can reveal which spin is scattered more. Increasing H causes the

phasors to rotate counterclockwise. The Landau level with electron magnetic moment down has the higher energy for a given quantum number and will be the first through the Fermi surface with increasing H. If $90° < \Phi < 180°$, as is the case here, $2\theta_1'$ $-\theta_2'$ will change by $180°$ as the SSA varies from zero to total. For intermediate values of SSA, the sign of the change will depend upon which spin is scattered more. As Fig. 14 shows, R_1 will be rotated clockwise (CW) and R_2 will be rotated counterclockwise (CCW) if the first level through the Fermi surface is scattered more. Thus,

$$(2\theta_1' - \theta_2')_{\text{SSA}} < (2\theta_1' - \theta_2')_{\text{no SSA}}$$

if the moment *down* electrons are scattered more, and

$$(2\theta_1' - \theta_2')_{\text{SSA}} > (2\theta_1' - \theta_2')_{\text{no SSA}}$$

if the moment *up* electrons are scattered more. In Cu-Fe, $2\theta_1' - \theta_2'$ was $-150°$ compared to $-45°$ for pure Cu; thus the moment *down* electrons were scattered more.

C. Comparisons with other measurements

Coleridge, Scott, and Templeton (CST)[4] have made extensive measurements in Cu with a variety of magnetic impurities using a dHvA spin-split-zero technique. The accuracy of their results was limited in Cu-Fe by its large SSA and relatively small value of H_{ex}. The combination of these two factors causes the spin-split zero to vanish before its angular position changed significantly. The CST measurements for a neck orbit at 50 kG are compared with values extrapolated to 50 kG from this work in Table II. The values found by CST and those of this experiment are in reasonable agreement considering the large uncertainties of their measurements and considering that the CST results are at angles away from symmetry direction. The orientation difference is important, since the interaction with the impurity is believed to be proportional to the amount of d wave contained in the orbit,[4] which varies with orientation. The CST value of H_{ex} is not concentration independent. The smaller H_{ex} per ppm found in the 93-ppm sample is consistent with the trend seen by CST and may indicate some impurity clustering.

CST also found qualitatively that the SSA doubled

TABLE II. Comparison between the values of δ_χ and H_{ex} from Coleridge and Templeton (Ref. 17) and this work.

	Fe (ppm)	δ_χ (°K/ppm)	H_{ex} (kG/ppm)
Coleridge and	6	0.0051	0.23
Templeton (Ref. 17)	22	0.0038	0.13
This work	93	0.0042	0.073

in going from 50 to 100 kG. They interpreted this as an indication that the Kondo state was being broken up by the magnetic field. However, another interpretation seems more reasonable.

Mössbauer measurements[22] in Cu-Fe indicate the polarization $\langle S_z \rangle$ of the Fe moment is linear with the field well above 50 kG, and does not approach saturation until well above 100 kG. The Fe impurity has a small moment ($\sim 1\mu_B$) at $1°$K, being well compensated by the Kondo state. Any breakup of the Kondo state would increase the moment, and make $\langle S_z \rangle$ saturate very rapidly. The fact that $\langle S_z \rangle$ continues to increase linearly with field indicates the Kondo state is still intact. The usual estimates for the field necessary to break up the Kondo state in Cu-Fe is $H_K \sim kT_K/\mu_B$, which ranges from 100 to 300 kG depending on the estimate of T_K used. For example, Mössbauer studies[22] give H_K ~ 235 kG, well above the 50 kG used in this experiment.

Simpson and Paton[23] (SP) have investigated the influence of the Kondo effect on dHvA measurements. They derive an expression for δ_χ in terms of the usual Kondo parameters:

$$k_B \delta_\chi = 2cJ^2 \rho \langle S_z \rangle (1 + \ln \text{ term}),\qquad(17)$$

where c is the impurity concentration in ppm, ρ is the conduction-electron density of states, and J is the strength of the exchange interaction. (SP use a term δ which is a symmetric, dimensionless quantity describing the SSA. The term δ_χ used here is the difference between the spin-up and -down scattering temperatures and has the dimensions of $°$K.) Fenton[24] in his comments on a similar paper by Miwa[25] objects to the inclusion of the logarithmic term on the basis that when higher-order processes are included, the logarithmic term vanishes. However, the logarithmic term introduces only at most a factor of 2, and is slowly varying with field and temperature used for these measurements in the range of this experiment. Our result that δ_χ varies linearly with H, therefore, demonstrates that the $\langle S_z \rangle$ term dominates the field dependence.

Fenton, SP, and Miwa agree that H_{ex} also ought to scale with $\langle S_z \rangle$ (the differences between them concern the logarithmic term). SP give

$$\mu_B H_{\text{ex}} = cJ \langle S_z \rangle (1 + \ln \text{ term}).\qquad(18)$$

From the Mössbauer data $\langle S_z \rangle$ is about 0.2 at 45 kG. Using (H_{ex} at 45 kG) = 6.1 kG (Table I) and neglecting the logarithmic term gives $J = -1.9$ eV.[26] It is interesting to compare this value with J_R determined from resistivity. J and J_R are not equivalent since J_R is a result of transport properties, but J from the dHvA effect is a measure of a static property. CST make use of this to interpret their results. They take $J_R = J/(2l+1) = J/5(l=2$ for d conduction electrons). Additionally, the value of

J must be weighted by the proportion of d waves in the neck orbit. The neck is a mixture of d and p waves, and only the d part has the appropriate symmetry to interact with the impurity. CST give a value for the square of the d wave amplitude of about 0.6. The value of J_R that may be compared with resistivity is thus

$$J_R = \frac{(-1.9 \text{ eV})}{(0.6)(5)} = -0.64 \text{ eV} .$$

The value from resistivity data is -0.7 eV,[20] which is in fortuitous agreement considering the uncertainties of the approximation.

The d-wave corrected value of J is -3.2 eV for Fe in Cu. CST found a value of -5.9 eV for Cu-Cr. Other measurements find that J for Cr is less than J for Fe. However, the results are not totally comparable. The CST value comes from an average over several orbits and under conditions of a nearly saturated moment. The Cu-Cr measurement was made near its Kondo temperature T_K while the Cu-Fe measurement was made well below T_K. The value of 0.2 for $\langle S_z \rangle$ may also be subject to considerable error, since the value is based upon extrapolated values of the saturated Mössbauer hyperfine field. The situation is complicated further by possible modification of the Kondo state above 100 kG, so the value of $\langle S_z \rangle$ must be regarded as only an estimate. There is also nothing in Kondo's theory that requires J to be temperature independent. Other determinations of J require the temperature dependence of a physical property, so there is an implicit averaging of J. dHvA experiments provide an opportunity to observe J as a function of T, but the experiment must be done in a system with $T_K \sim 1$ °K so that a sufficient temperature range can be covered to expect a change in J and still be able to observe the dHvA effect.

D. SSA and theoretical approximations

The connection between SSA and the parameters (energy and width) of the impurity level has not been clearly discussed in the literature. Although several authors have incorporated SSA in magnetoresistance calculations,[27,28] only SP derive a result pertinent to the dHvA effect. However, their work was within the domain of the s-d exchange model, and does not contain enough of the impurity level's properties even to account for the range of behavior observed in Cu alloys. This is readily demonstrated. No measurable SSA is observed in Cu-Cr ($T_K \sim 1$ °K) while Cu-Mn ($T_K \sim 0.1$ °K) and Cu-Fe ($T_K \sim 10$ °K) have considerable SSA. Using Eqs. (17) and (18), a convenient ratio for the comparison of relative amounts of SSA is

$$\frac{\delta_X}{H_{\text{ex}}} = \frac{\mu_B}{k_B} \frac{2cJ^2\rho\langle S_z\rangle(1+\ln \text{ term})}{cJ\langle S_z\rangle(1+\ln \text{ term})} .$$

This ratio is independent of the impurity concentration, $\langle S_z \rangle$, and the disputed logarithmic term. For a given host metal, it should only depend on the size of the exchange integral J for the specific impurity. According to estimates of SP, the quantity δ_X/JH_{ex} ought to be the same for Cu-Cr, Cu-Mn, and Cu-Fe. However, using values of δ_X and H_{ex} from CST and this work, and an average J as measured from a variety of physical properties,[1] an estimate of the parameter δ_X/JH_{ex} for the impurities Cr, Mn, and Fe give values of 0.00, 0.02, and 0.06, respectively. Clearly, this expression is not constant and the work of SP must omit an important term. More theoretical work is required to understand the difference between these impurity systems.[26]

V. CONCLUSIONS

dHvA waveshape analysis is a powerful tool for investigating the details of the electron-impurity interaction. The information available from this technique (scattering rate, spin scattering anisotropy, and g factor) compliments the information available from bulk microscopic and macroscopic measurements. The techniques described here make possible meaningful and precise waveshape measurements, even in the presence of complicating experimental conditions.

The simple relations between H_{ex}, δ_X, and $\langle S_z \rangle$ demonstrated in this work offer some encouragement that theoretical progress in this problem is possible. The specific quantities measured here should be simpler to relate to fundamental calculations than bulk-property measurements, and may provide a direct check for various models and methods of calculation.

APPENDIX

Suppose the field range is restricted so that first-order equations in H or $1/H$ are sufficient to de-

scribe the data. Then the theoretical quantities
(Q) will be defined to first-order (linear) field de-
pendence, and can be simply expressed in terms of
values at two field points, H_1 and H_2, using the
equation

$$Q(H) = Q_0 + bH \ ,$$

where

$$b = \frac{Q(H_2) - Q(H_1)}{H_2 - H_1}$$

and

$$Q_0 = Q(H_1) - bH_1 \ .$$

Using this relation and Eqs. (3), (4), and (7) the
following equations for the measured quantities
in terms of the theoretical quantities may be de-
rived

$$2\theta_1 - \theta_2 = 2 \tan^{-1}\left[\tan(\Phi/2)\left(\frac{1-A}{1+A}\right)\right]$$

$$- \tan^{-1}\left[\tan(\Phi)\left(\frac{1-A^2}{1+A^2}\right)\right], \qquad (A1)$$

$$\ln\left(\frac{R_2}{R_1}\right) = \ln\left(\frac{B(1+A^4+2A^2\cos2\Phi)^{1/2}}{(1+A^2+2A\cos\Phi)^{1/2}}\right), \qquad (A2)$$

$$\beta = \frac{d}{d(1/H)}\left[\ln\left(\frac{R_2}{R_1}\right)\right]$$

$$= R_1\frac{dR_2}{d(1/H)} - R_2\frac{dR_1}{d(1/H)}\Big)\Big/R_1R_2 \ , \qquad (A3)$$

where

$$\frac{dR_1}{d(1/H)} = \frac{R_1}{B}\frac{dB}{d(1/H)}$$

$$+\frac{B^2}{R_1}\left[(A - \cos\Phi)\frac{dA}{d(1/H)}\right.$$

$$\left. - A\sin\Phi\frac{d\Phi}{d(1/H)}\right]$$

and

$$\frac{dR_2}{d(1/H)} = \frac{2R_2}{B}\frac{dB}{d(1/H)}$$

$$+\frac{B^4}{R_2}\left[2(A^3+A\cos2\Phi)\frac{dA}{d(1/H)}\right.$$

$$\left. - 2A^2\sin2\Phi\frac{d\Phi}{d(1/H)}\right] \ ,$$

with

$$\frac{dB}{d(1/H)} = -\alpha\left(X_{H_1}^0 - \frac{X_{H_2}^0 - X_{H_1}^0}{H_2 - H_1}\right)B \ ,$$

$$\frac{dA}{d(1/H)} = -\alpha\left((\delta_x)_{H_1} - \frac{(\delta_x)_{H_2} - (\delta_x)_{H_1}}{H_2 - H_1}\right)A \ ,$$

and

$$\frac{d\Phi}{d(1/H)} = -\left(\frac{\Phi_{H_2} - \Phi_t'}{H_2 - H_1}\right)H_2 \ .$$

β is evaluated from the data using

$$\beta = \frac{\ln(R_2/R_1)_{H_2} - \ln(R_2/R_1)_{H_1}}{1/H_2 - 1/H_1} \ . \qquad (A4)$$

Since the $\ln(R_2/R_1)$ data is assumed to fit a *first-
order* equation in $1/H$, there is the additional con-
straint that $\beta_{H_1} = \beta_{H_2}$. Equations (A1), (A2), and
(A3) are valid for any field value provided A, B,
etc., are evaluated for the same field value.

[1] For a review, see A. J. Heeger, in *Solid State Physics*,
edited by F. Seitz and D. Turnbull (Academic, New
York, 1969), Vol. 23, pp. 283–411.
[2] D. H. Lowndes, K. Miller, R. G. Poulsen, and M.
Springford, Philos. Trans. R. Soc. Lond. A **331**, 497
(1973).
[3] P. T. Coleridge and I. M. Templeton, Phys. Lett. A
27, 344 (1968); Phys. Rev. Lett. **24**, 108 (1970).
[4] P. T. Coleridge, G. B. Scott, and I. M. Templeton,
Can. J. Phys. **50**, 1999 (1972).
[5] I. M. Lifshitz and A. M. Kosevich, Zh. Eksp. Teor.
Fiz. 29, 730 (1955) [Sov. Phys.-JETP **29**, 636 (1956)].
[6] P. T. Coleridge, J. Phys. F **2**, 1016 (1972).
[7] Y. K. Chang (unpublished).
[8] F. Haberda, master's thesis (University of Oregon,
1972) (unpublished).
[9] D. W. Terwilliger and R. J. Higgins, J. Appl. Phys.
43, 3346 (1972); Phys. Rev. B **7**, 667 (1973).
[10] The analysis was carried out at Bell Laboratories.
[11] H. G. Alles and R. J. Higgins, Rev. Sci. Instrum. **44**,
72 (1973).
[12] H. G. Alles and R. J. Higgins (unpublished).
[13] For example, see A. V. Gold, in *Solid State Physics*,
Volume 1, Electrons in Metals, edited by J. F. Coch-
ran and R. R. Haering (Gordon and Breach, New York,
1968).
[14] This function is briefly discussed in Ref. 13 and was
originally given by Johnson in a now unavailable AEC
document.
[15] This effect may be responsible for the amplitude anom-
aly reported by M. Springford, Adv. Phys. **20**, 493
(1971).
[16] D. Shoenberg, Phil. Trans. R. Soc. Lond. A **255**, 85
(1962).
[17] R. A. Phillips and A. V. Gold, Phys. Rev. **128**, 932
(1969).
[18] H. G. Alles, R. J. Higgins, and D. Lowndes (unpub-
lished).
[19] A preliminary report of some of these results has ap-
peared: H. G. Alles, R. J. Higgins, and D. H.

Lowndes, Phys. Rev. Lett. **30**, 705 (1973).

[20] M. D. Daybell and W. A. Steyert, Phys. Rev. Lett. **18**, 398 (1967).

[21] P. Monod, Phys. Rev. Lett. **19**, 1113 (1967).

[22] R. B. Frankel, N. A. Blum, Brian B. Schwartz, and Duk Joo Kim, Phys. Rev. Lett. **12**, 105 (1967).

[23] G. Simpson and B. E. Paton, Phys. Lett. A **34**, 180 (1971).

[24] E. W. Fenton, Solid State Commun. **10**, 185 (1972).

[25] H. Miwa, T. Ando, and H. Shiba, Solid State Commun. **8**, 2161 (1970).

[26] Since this paper was submitted a calculation of ϵ_{ex} for the Kondo ground state (appropriate for Cu-Fe) has been brought to our attention. See: K. Yosida and A. Yoshimori, in *Magnetism* V, edited by G. Rado and H. Suhl, (Academic, New York, 1973). The ln term is replaced by $(1 + J\rho/N)$ in the ground-state limit, and $\langle S_z \rangle$ is the *effective* moment at the particular value of H. The estimate of J given in the text (based on the exchange scattering models, e.g., Ref. 23) is not substantially altered, since $|J\rho/N| \simeq 0.1$, i.e., $(1 + J\rho/N) \simeq 1$. However, recently Shiba has completed a substantially improved calculation of the dHvA effect in the presence of magnetic impurities which is not limited to the perturbation regime (i.e., is applicable to Cu-Fe), and which takes into account the differing properties of different impurities in a way which explains the discrepancy in the Simpson—Paton calculation noted in Sec. IV of the text. In particular, potential scattering is included, and the magnitudes of theoretical parameters (in particular J) to be obtained from the measured ϵ_{ex} and SSA are altered. See: Hiroyuki Shiba, J. Theor. Phys. (to be published). We are grateful to Y. Yoshimori, H. Shiba, and E. Fenton for bringing this recent work to our attention.

[27] R. More and H. Suhl, Phys. Rev. Lett. **20**, 500 (1968).

[28] M. T. Beal-Monod and R. A. Weiner, Phys. Rev. **170**, 552 (1968).